The dependence of uniform momentum zones on mean shear and turbulence intensity

R. Jason Hearst[1,2]

[1]Department of Energy and Process Engineering
Norwegian University of Science and Technology
Trondheim, Norway
r.j.hearst@southampton.ac.uk

Bharathram Ganapathisubramani[2]

[2]Engineering and the Environment
University of Southampton
Southampton, United Kingdom
g.bharath@southampton.ac.uk

ABSTRACT

The influence of mean shear and turbulence intensity on the existence and population of uniform momentum zones (UMZs) in shear flows is investigated experimentally with hot-wire anemometry and particle image velocimetry. UMZs have typically been investigated in wall-bounded flows (Adrian *et al.*, 2000; Kwon *et al.*, 2014; de Silva *et al.*, 2016) and have been associated with the hierarchy of eddy packets that often present as hairpin-like structures. Similar structures have also been observed in uniform shear turbulence (Vanderwel & Tavoularis, 2011) and homogeneous shear turbulence (Dong *et al.*, 2017). Thus, it is likely that UMZs exist in these flows as well. Investigating UMZs away from the wall provides benefits in that a wide range of parameters can be tested. For instance, in a boundary layer, the turbulence intensity and mean profile are relatively fixed. However, in a wind tunnel shear flow the shear and turbulence intensity can be varied independently of one another. This is achieved here with an active grid. Four test cases are produced. Two have comparable turbulence intensity, but different linear shear. A third profile has similar turbulence intensity and centreline shear parameter, but the profile is non-linear. The final profile has linear shear within the range of the other profiles, but substantially different turbulence intensity. UMZs are detected in all four flows using modal velocities detected from instantaneous probability density functions of the streamwise velocity (Adrian *et al.*, 2000; de Silva *et al.*, 2016). For the cases where the turbulence intensity was comparable, but the shear was varied, it was found that the distribution of modal velocities and the number of UMZs did not vary significantly. In contrast, when the turbulence intensity is increased, then the distribution of modal velocities becomes wider and it becomes more likely to observe a higher number of UMZs in each velocity field. The present results indicate that the population of UMZs is a function of turbulence intensity rather than shear for the cases investigated here. This observation supports the finding of de Silva *et al.* (2016) that the number of UMZs increases with Reynolds number because the local turbulence intensity in the log-layer of wall-bounded flows also increases with Reynolds number.

INTRODUCTION

Instantaneously, a turbulent boundary layer (TBL) is composed of layered regions of approximately uniform momentum (Meinhart & Adrian, 1995; Adrian *et al.*, 2000). These regions have become known as 'uniform momentum zones' (UMZs) and a detailed investigation of them in TBLs was performed by de Silva *et al.* (2016). UMZs are separated by strong shear events that represent jumps in the velocity and energy. It would appear that the phenomenon of packets of fluid being separated by strong shear events is ubiquitous across flows. For instance, in direct numerical simulations (DNS) of periodic box turbulence with homogeneous forcing, Ishihara *et al.* (2013) found that complex thin shear layers separate vorticity events. Similar findings were made by Fiscaletti *et al.* (2016) in DNS of a mixing layer.

In recent years, it has become apparent that many of the features often associated with wall-bounded flows can be reproduced in other shear flows. With DNS, Mizuno & Jiménez (2013) and Sekimoto *et al.* (2016) demonstrated that statistically stationary homogeneous shear turbulence can be used to recover the log-layer behaviour of a TBL. Using hydrogen bubbles and particle image velocimetry (PIV), Vanderwel & Tavoularis (2011) identified that hairpin-like structures exist in uniform shear flows. More recently, the DNS study of Dong *et al.* (2017) provided further evidence that similar instantaneous structures are found in both wall-bounded flows, and homogeneous shear turbulence where the wall could not have given rise to the structure.

Given that homogeneous and uniform shear flows manifest similar characteristics and structures to a TBL, it suggests that such flows could be used to gain further insight on UMZ phenomenology. In particular, do UMZs exist in a generic shear flows, and if so, can we learn something about their behaviour in general from such flows? For instance, does the number of UMZs (N_{UMZ}) depend on the shear or turbulence intensity? Do the modal velocities associated with the UMZs have a dependence on the shear or turbulence intensity? Do UMZs only manifest in shear profiles with non-linear gradients, like a boundary layer, or can they materialize in linear shear? Addressing these issues is difficult in a TBL where the main flow parameters remain roughly fixed by the wall and Re_τ. Thus, one cannot easily ascertain the (possibly) independent effects of shear and turbulence intensity on the population and existence of UMZs. In this study, we devise a set-up to investigate UMZ populations in the presence of controllable shear and turbulence intensity in wind tunnel turbulent shear flows. The goal is to ascertain if UMZs appear in such flows, and if they do, what the effects of shear and turbulence are on the populations.

EXPERIMENTAL DETAILS

An active grid was used to generate shear profiles and measurements were performed with hot-wire anemometry and PIV independently. The experimental campaign was conducted in the 0.9 m $\times$ 0.6 m $\times$ 4.5 m suction wind tunnel at the University of Southampton. The active grid was placed at the test-section inlet and was operated in four different patterns to create a variety of mean shear and turbulence intensity profiles. The active grid features an array of 11 vertical bars and 7 horizontal bars with square wings mounted to them. These bars are actuated by stepper motors. The mesh length, M, of the grid is 81 mm; see Dogan *et al.* (2016) for more details on this device. The grid was operated by flapping the vertical bars through different angles to create varying blockage across the test-section in order to control the mean shear level. The horizontal bars were operated in the 'fully random' mode described by Hearst & Lavoie (2015), and were used to control the turbulence level.

The hot-wire measurements were performed $41.3M$ downstream of the grid by traversing across the shear direction (the y-axis). Four single-wires mounted to a profiled rake were sam-

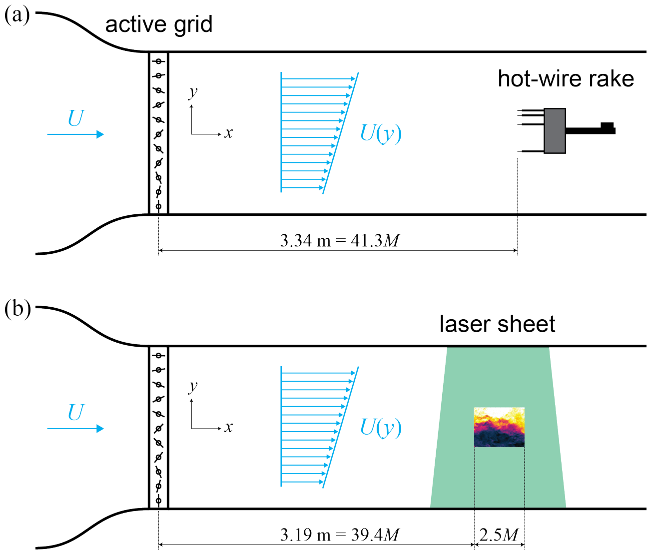

Figure 1. Illustrative schematic of the experimental set-up for the (a) hot-wire anemometry measurements and (b) the particle image velocimetry measurements. Not to scale.

pled simultaneously. A schematic of the hot-wire set-up is provided in Fig. 1(a). All wires were made in-house from tungsten wire mounted to Dantec-style prongs. Copper plating was used to isolate the sensing lengths, which were nominally maintained at $\ell = 1$ mm for all wires. The hot-wire probes were operated by a Dantec 54N82 multi-channel constant temperature anemometer, and the signals were acquired at 20.5 kHz with an analogue filter at 10 kHz. A National Instruments USB-6212 16-bit data acquisition card was used to capture the voltage signals. Data were acquired for six minutes, resulting in the acquisition of 7000 centreline eddy turn-overs for the worst-case. Calibrations were performed *in situ* by fitting a fourth-order polynomial to at least 15 points. The spatial resolution of the hot-wire probes is provided in Table 1 relative to the Kolmogorov microscale, $\eta = \nu^{3/4}/\langle\varepsilon\rangle^{1/4}$, where ν is the kinematic viscosity and $\langle\varepsilon\rangle = 15\nu\langle(\partial u/\partial x)^2\rangle$ is the mean dissipation rate of turbulent kinetic energy. With the hot-wire, spatial gradients were computed using Taylor's frozen flow hypothesis, i.e., $(\partial/\partial t) = U(\partial/\partial x)$. Gradients were estimated with a sixth-order central-differencing scheme in order to balance the accuracy of the method with the noise level of the hot-wire (Hearst *et al.*, 2012). The subscript $\cdot_0$ denotes a quantity along the centreline throughout this work.

PIV snapshots were acquired with two adjacent LaVision ImagerProLX 16 mega-pixel cameras equipped with Sigma 105 mm lenses and Kenko 1.4× teleconverters. The field-of-view (FOV) spanned from 39.4M to 41.9M, thus encompassing the hot-wire measurement axis. A schematic of the PIV set-up is provided in Fig. 1(b). A fog generator was used to produce smoke particles with a nominal diameter of 1 μm. The particles were illuminated by a Litron Lasers Nano PIV laser (Nd-YAG, 532 nm, 200 mJ). Two thousand five hundred image pairs were acquired of the 203 mm × 165 mm FOV. The time between images in a pair was $\Delta t = 70$ μs, and image pairs were acquired at 0.6 Hz, thus ensuring each vector field was independent. The vector fields were processed with LaVision DaVis 8.3 using multiple passes starting with a 128 × 128 window with 50% overlap and progressing down to a 24 × 24 window with 75% overlap. The resolution of an interrogation window was typically between $4\eta_0$ and $5\eta_0$ and is provided in Table 1 as $\Delta x/\eta_0 \times \Delta y/\eta_0$.

FLOW CHARACTERISTICS

Four active grid control sequences were used to produce different turbulent shear flows. All four profiles were acquired at $Re_M = U_0 M/\nu \approx 53{,}000$. The flow parameters for each case are provided in Table 1. In the present study, the dimensional shear parameter (units of m^{-1}) is used to describe the mean velocity gradient (Nedić & Tavoularis, 2016),

$$k_s = \frac{1}{U_0}\frac{\partial U}{\partial y}, \tag{1}$$

and is provided in Table 1 for all cases. The $\partial U/\partial y$ gradient is estimated from a linear fit to $-1 \le y/M \le +1$. The table also includes estimates of the turbulent Reynolds number based on the Taylor microscale, given by

$$Re_\lambda = \frac{u'\lambda}{\nu}, \tag{2}$$

where u' is the standard deviation of the velocity fluctuations and λ is the Taylor microscale,

$$\lambda^2 = \frac{\langle u^2\rangle}{\langle(\partial u/\partial x)^2\rangle}. \tag{3}$$

The approximate size of the large scales is estimated from the integral scale given by the integral of the autocorrelation of the velocity fluctuations to the first zero-crossing. The shear and turbulence intensity were deliberately varied for each case, while the other parameters listed in Table 1 are dependent variables.

Fig. 2 shows the mean velocity and turbulence intensity profiles measured with both the hot-wire rake and PIV. In general, there is good agreement between the two measurement techniques for the mean velocity, and similar trends are observed for the turbulence intensity. The overestimation of the turbulence intensity by PIV is typical, and is a result of higher noise relative to the hot-wire signal.

Cases A and C have similar turbulence intensity profiles and differ only in that the mean velocity profile of A is linear whilst the profile of C is non-linear; this is particularly evident for $y/M < 0$ in Fig. 2(a). Both these cases are comparable to case B that has marginally higher turbulence intensity ($u'_0/U_0 + 1.4\%$), but a 46% change in k_s. These cases can then all be compared to case D, which has k_s within the range spanned by A, B, and C, but significantly higher turbulence intensity, 13.9% compared to 10.2% for case B and 8.8% for cases A and C.

These four cases allow for the investigation of several questions pertaining to the existence and population of UMZs in shear flows. First, if all turbulence parameters are kept constant, but a linear profile is compared to one with curvature (like in a boundary layer), does the population of UMZs change? Second, if the turbulence intensity is held constant (or allowed to vary marginally, e.g., between cases A and B), are the UMZs affected? Lastly, what is the impact of significantly increasing the turbulence intensity? The remainder of this work endeavours to address these questions.

DETECTION OF UNIFORM MOMENTUM ZONES

UMZs manifest as instantaneous packets of similar momentum (or velocity) that are separated by strong shear events. Their detection has been previously detailed by Adrian *et al.* (2000) and de Silva *et al.* (2016), and includes the identification of modal velocities in the instantaneous velocity field associated with peaks in

Table 1. Flow parameters. Length scales, turbulence intensities, Reynolds numbers and hot-wire resolution were evaluated with the hot-wire data. All other parameters are from the PIV measurements.

Case	Symbol	Colour	U_0 [m s^{-1}]	u'_0/U_0 [%]	k_s [m^{-1}]	$Re_{\lambda,0}$	η_0 [mm]	λ_0 [mm]	L_0 [mm]	$\overline{N}_{\mathrm{UMZ}}$	ℓ/η_0	$\Delta x/\eta_0 \times \Delta y/\eta_0$
A	○	black	10.2	8.8	1.12	474	0.20	8.4	179	1.85	5.1	4.1×4.1
B	□	red	10.1	10.2	0.60	501	0.18	7.7	324	1.86	5.7	4.6×4.6
C	◊	blue	10.2	8.8	1.05	505	0.21	9.1	154	1.86	4.9	3.9×3.9
D	▲	green	10.3	13.9	0.89	701	0.15	7.9	513	2.21	6.6	5.3×5.3

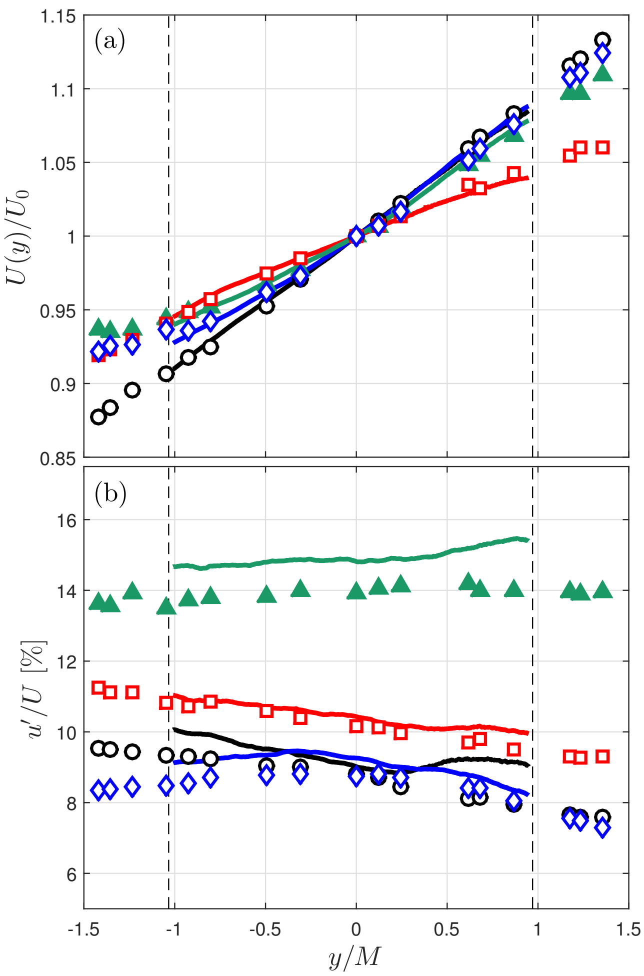

Figure 2. Mean profiles of the (a) streamwise velocity and (b) turbulence intensity for the four shear cases. The symbols represent hot-wire measurements whilst the lines represent PIV measurements. The vertical dashed lines represent the edges of the PIV interrogation domain. See Table 1 for legend.

the instantaneous streamwise velocity histogram. The application of this concept is only relevant if the flow is in fact divided into regions of approximately uniform momentum. While a boundary layer may have some underlying organisation that manifests into these regions divided by shear, it has not yet been demonstrated that the same would be true in a flow with a linear velocity gradient uninfluenced by the boundary condition of the wall.

The process used for UMZ detection here is illustrated in Fig. 3 and 4. Fig. 3(a) shows an instantaneous velocity profile for case D compared to the mean profile. It is apparent that the instantaneous profile is composed of significant variations in the velocity, and that only once a large number of samples are averaged does a smooth profile emerge. The corresponding instantaneous flow field for the profile in Fig. 3(a) is provided in Fig. 3(c). The probability density function (PDF) of all streamwise velocities that appear in this FOV is the red line in Fig. 4. This PDF has several peaks that are taken to represent modal velocities associated with the bulk motion of UMZs. In highly turbulent flows, the instantaneous PDF of velocities is smoothed by the fluctuations. To combat this and isolate the background large scales, we spatially filter the flow with a $\lambda_0 \times \lambda_0$ Hanning window. The filter size was chosen based on a flow scale so that its influence was similar for all cases. The Taylor microscale was chosen in particular because it represents an intermediate scale, and thus the bulk should be preserved while the fluctuations are filtered. The filtered velocity field is shown in Fig. 3(b), and the corresponding profile and histogram are represented by the black lines in Fig. 3(a) and Fig. 4. Interestingly, while the profile is smoothed by filtering, the PDF is more jagged, thus emphasizing the peaks and facilitating the detection of modal velocities. For the worst-cases, the mean shear $(\partial U/\partial y)$ changed by 1.4% while the mean centreline velocity (U_0) changed by 0.5% between unfiltered and filtered cases. The turbulence intensity from PIV was attenuated by approximately 1.5% across the profiles. Thus, the flow physics were generally preserved while the flow field was smoothed to make the background flow more pronounced.

The filtered velocity profile in Fig. 3(a) traces the same path as the raw profile but without the fluctuations. The location where the UMZ boundaries intersect the profiles are represented in Fig. 3(a) with horizontal dashed lines. It is evident that the UMZ edges are located in regions of high shear, and are separating areas of approximately uniform momentum. Tracing the UMZ boundaries onto the map of the normalised instantaneous shear, Fig. 3(d), shows that they effectively connect the shear events in the flow (Meinhart & Adrian, 1995; Adrian *et al.*, 2000; Eisma *et al.*, 2015; de Silva *et al.*, 2016) and surround areas that are relatively shearless. Thus, the above provides confidence that the methodology used herein identifies UMZs, and that this approach may be applied to each data set to determine if the flow characteristics impact the UMZ populations.

Before departing this section, it is worth commenting on the chosen investigation window for UMZ detection. A square of size $0.08/k_s \times 0.08/k_s$ was selected so that matched fields-of-view based on the flow parameters were used. When the shear parameter is multiplied by a distance, it represent the total strain to that point. This is the relevant large scale spatial normalisation in shear flows (Vanderwel & Tavoularis, 2011; Nedić & Tavoularis, 2016). It is akin to

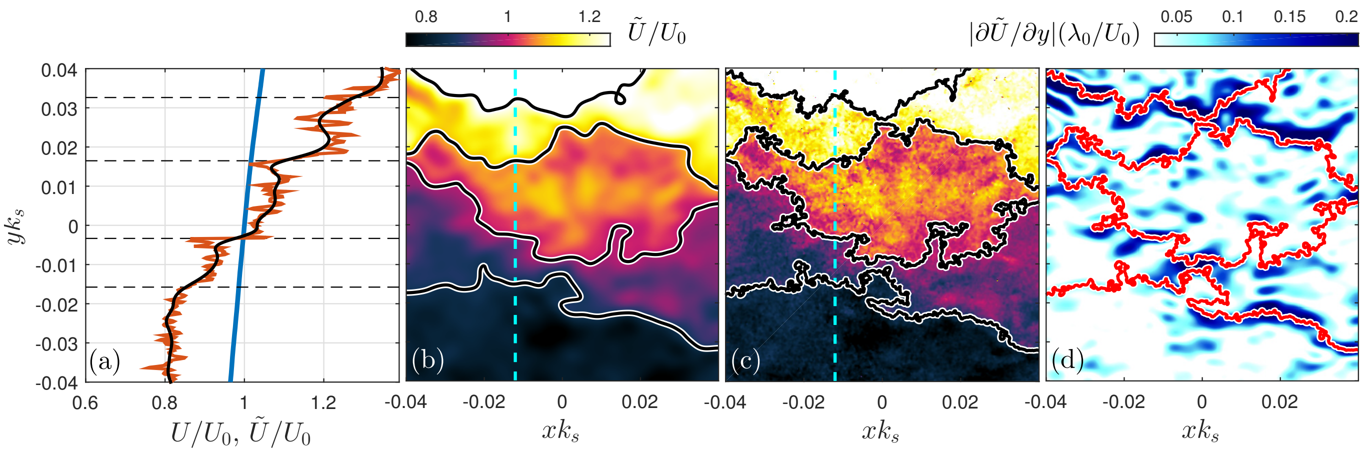

Figure 3. Sample instantaneous velocity field from case D. Velocity profiles are shown in (a) where the blue line is the mean velocity profile, the red line is the instantaneous profile, and the black line is the instantaneous velocity profile from the $\lambda_0 \times \lambda_0$ filtered velocity field. The dashed horizontal lines represent where the UMZ limits intersect the profiles. The instantaneous velocity field filtered at $\lambda_0 \times \lambda_0$ is shown in (b), with UMZ limits drawn as solid lines. The true instantaneous velocity field is provided in (c), and the instantaneous shear field is provided in (d). The dashed vertical lines in (b) and (c) are the location of the instantaneous profiles in (a).

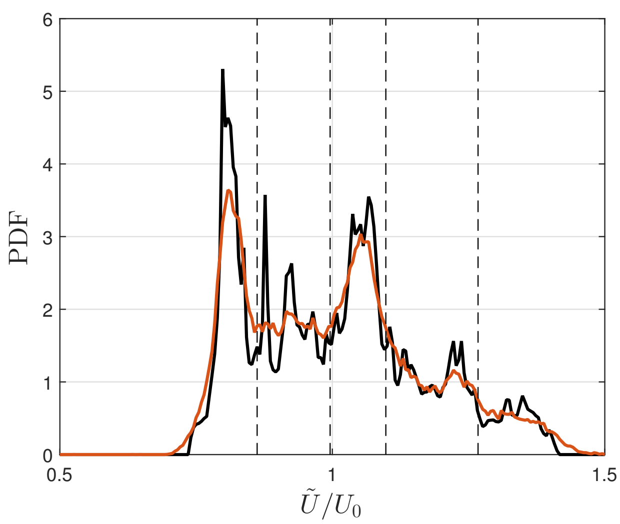

Figure 4. Probability density functions of the instantaneous streamwise velocity from the field examined in Fig. 3. The black line is from the filtered velocity field (Fig. 3(b)), and the red line is from the raw velocity field (Fig. 3(c)). The vertical dashed lines represent the thresholding levels between UMZs.

using a non-dimensionalisation based on δ in a boundary layer. The size of the square was chosen to maximize the FOV, while maintaining the same normalised size for all cases. de Silva *et al.* (2016) suggested that the relevant length scale for UMZ investigation should in fact be one based on viscous units rather than the large scales. They highlighted that a viscous unit based limit could be set to detect smaller UMZs, while a large scale limit biases the analysis to detection of only larger UMZs. de Silva *et al.* (2016) suggested a limit of 2000 viscous units, but found that the mean number of zones detected did not vary significantly for a wide range of fields-of-view ranging from 250 to 2500 viscous units. The relevant viscous unit in the present flow is the Kolmogorov microscale, and our UMZ investigation domains, that are fixed relative to k_s, vary from $365\eta_0$ to $770\eta_0$. Thus, the present investigation windows are within the range that de Silva *et al.* (2016) found no significant impact of FOV on the number of detected UMZs.

UNIFORM MOMENTUM ZONE STATISTICS

The methodology described in the previous section was applied to all four data sets, providing insight on the influence of the changing shear and turbulence parameters on the population of UMZs. Fig. 4 shows a PDF of the modal velocities accumulated over all images for each case. Of note is that cases A, B and C are well collapsed. This indicates two things: (1) there is no significant impact on the distribution of modal velocities for a significant change in k_s if u_0'/U_0 is relatively constant (compare cases A and B); (2) maintaining a similar k_s but adding curvature similarly does not appear to have a significant effect on the distribution of modal velocities (compare cases A and C). However, a significant impact on the distribution of modal velocities is felt when the turbulence intensity is increased (compare case D to all other cases). Increasing u_0'/U_0 widens the tails of the PDF of modal velocities, identifying that UMZs with more extreme modal velocities occur more frequently.

A secondary feature of interest with respect to the distribution of modal velocities in Fig. 5 is that they are approximately symmetric about U_0 for all cases. This contrasts with similar PDFs composed in TBLs (de Silva *et al.*, 2016) or turbulent channel flow (Kwon *et al.*, 2014) where there is a bias of the modal velocities to the free-stream or 'quiescent core', respectively. This is significant for multiple reasons. The zero velocity near the wall in both wall-bounded flows is likely the culprit for this bias as the present experiment does not have a zero velocity region within the investigation domain. Secondly, it is unlikely that the bias is due to the changing gradient because there is no difference in Fig. 5 between our linear and curved profiles. Lastly, it is possible that spatial resolution contributes to the perceived bias in wall-bounded measurements. The local viscous length scale changes with wall-normal position in wall-bounded flows, effectively resulting in better spatial resolution farther from the wall, whereas in the present flow η changes by $\pm 3\%$ in the worst-case across the PIV domain, resulting in relatively constant spatial resolution relative to the local viscous scales.

Another statistic of interest is the number of detected UMZs

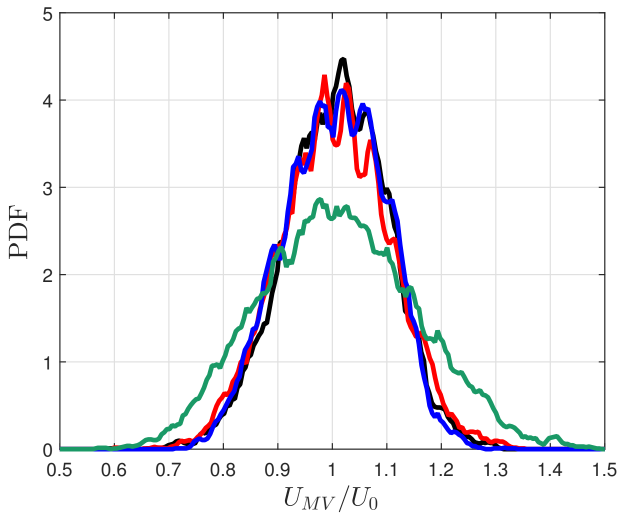

Figure 5. Probability density functions of the modal velocities accumulated from all vector fields for each case. See Table 1 for legend.

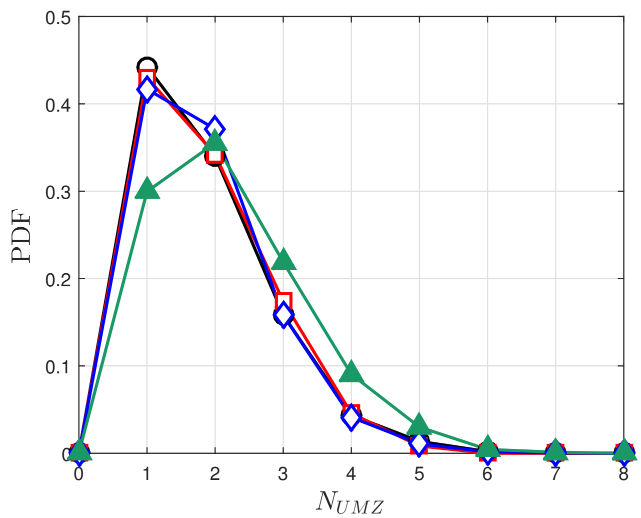

Figure 6. Probability density function of the number of UMZs detected for each shear case. See Table 1 for legend.

(N_{UMZ}). The PDF of N_{UMZ} for each case is given in Fig. 6 and the mean value of N_{UMZ} is provided in Table 1. Like the results for the modal velocities, there is no significant difference between cases A, B, and C. For these three cases, it is most likely that $N_{\mathrm{UMZ}} = 1$, i.e., there is only one peak present and thus it is difficult to ascertain if there are any UMZs. However, there are still net more fields where $N_{\mathrm{UMZ}} > 1$, identifying that it is more likely there are UMZs than that there aren't. Interestingly, when the turbulence intensity is increased for case D, the PDF changes and N_{UMZ} grows. For case D, $\overline{N}_{\mathrm{UMZ}} > 2$ and it is more likely that $N_{\mathrm{UMZ}} = 2$ than that there are no UMZs.

The cumulative statistics thus paint a picture of the influence of mean shear and turbulence intensity on the distribution of UMZs in turbulent shear flows. It appears that both the amount of shear, and its curvature do not significantly influence the number of UMZs detected or their modal velocities. In contrast, when the turbulence intensity is increased significantly, there is an increase in the number of UMZs detected and the distribution of modal velocities is wider.

DISCUSSION

A natural question arising from the above is: how can these results be related to measurements of UMZs in TBLs and channel flow? A primary finding of de Silva *et al.* (2016) was that there was a log-linear relationship between Re_τ and $\overline{N}_{\mathrm{UMZ}}$, that resulted in $\overline{N}_{\mathrm{UMZ}}$ increasing with Re_τ. Following arguments initially presented by Adrian *et al.* (2000), de Silva *et al.* (2016) suggested that the increase in $\overline{N}_{\mathrm{UMZ}}$ with Re_τ is a result of hierarchical structures of packet eddies, that in turn have a log-linear increase with Re_τ. They supported this hypothesis with results from the attached eddy model. Here, we see that $\overline{N}_{\mathrm{UMZ}}$ increases with increasing turbulence intensity. Interestingly, the turbulence intensity in the plateau region and log-layer of a TBL also increases with Re_τ (Hutchins *et al.*, 2009). Thus, in boundary layers there is also a relationship between an increase in turbulence intensity and $\overline{N}_{\mathrm{UMZ}}$, and these two sets of results would seem to corroborate one another.

This has interesting ramifications for the structure of the flow and possible extensions to coherent structures. Adrian *et al.* (2000) draw clear ties between UMZs and the passage of hairpin-like structures. Given that increasing the turbulence intensity produces more UMZs in the same space relative to k_s, it suggests that the UMZs are themselves becoming thinner relative to k_s. This may represent an increase in the number of eddy packets as observed in boundary layers for increasing Re_τ. The overarching theme is that these parameters increase as a result of increasing turbulence intensity.

CONCLUSIONS

An active grid was used to generate bespoke turbulent shear profiles in order to investigate uniform momentum zones in generic shear flows. Three profiles were produced with approximately the same turbulence intensity ($u'_0/U_0 \pm 0.7\%$). Two of these cases had linear shear with very different shear parameters, k_s, while the third matched k_s and u'_0/U_0 to another case, but had a non-linear profile. These cases were then compared to a fourth case with comparable k_s, but a significantly higher u'_0/U_0.

It was found that UMZs do manifest in all four flows, however, for the three cases with similar u'_0/U_0 nearly 40% of the measured vector fields had no UMZs. It is significant though that in all cases there were more vector fields with two or more UMZs than ones without any UMZs. For the three cases where the shear profile was changed, but the turbulence intensity was held constant, there was no significant change to the structure of the UMZs. The modal velocities identified (i.e., the velocities associated with the UMZs), the average number of UMZs, and the distribution of the number of UMZs was functionally the same for these three cases. In contrast, when the turbulence intensity was increased, the distribution of modal velocities became wider, the number of UMZs increased, and it became more common to see two or more UMZs in an instantaneous vector field. The present results thus suggest that variations in UMZ population is a result of changes in the turbulence intensity, and not the shear.

In general, the local turbulence intensity increases in magnitude in a turbulent boundary layer as Re_τ increases (Hutchins *et al.*, 2009). This may be a contributing reason that de Silva *et al.* (2016) observed an increase in the number of UMZs with Re_τ. Conversely, if their connection between the number of UMZs and heirerchal eddy packets is correct, it may imply that there is a similar increase in the hierarchy of eddy packets in the shear flows investigated here.

ACKNOWLEDGEMENTS

The authors acknowledge the financial support of the European Research Council (ERC Grant agreement No. 277472), and the Engineering and Physical Sciences Research Council of the United

Kingdom (EPSRC Grant Ref. No. EP/I037717/1). RJH acknowledges the financial support of the Natural Sciences and Engineering Research Council of Canada (NSERC). BG acknowledges the financial support of the Leverhulme Trust.

REFERENCES

Adrian, R. J., Meinhart, C. D. & Tomkins, C. D. 2000 Vortex organization in the outer region of the turbulent boundary layer. *J. Fluid Mech.* **422**, 1–53.

de Silva, C. M., Hutchins, N. & Marusic, I. 2016 Uniform momentum zones in turbulent boundary layers. *J. Fluid Mech.* **786**, 309–331.

Dogan, E., Hanson, R. & Ganapathisubramani, B. 2016 Interactions of large-scale free-stream turbulence with turbulent boundary layers. *J. Fluid Mech.* **802**, 79–107.

Dong, S., Lozano-Durán, A., Sekimoto, A. & Jiménez, J. 2017 Coherent structures in statistically stationary homogeneous shear turbulence. *J. Fluid Mech.* **816**, 167–208.

Eisma, J., Westerweel, J., Ooms, G. & Elsinga, G. E. 2015 Interfaces and internal layers in a turbulent boundary layer. *Phys. Fluids* **27** (055103).

Fiscaletti, D., Attili, A., Bisetti, F. & Elsinga, G. E. 2016 Scale interactions in a mixing layer - the role of the large-scale gradients. *J. Fluid Mech.* **791**, 154–173.

Hearst, R. J., Buxton, O. R. H., Ganapathisubramani, B. & Lavoie, P. 2012 Experimental estimation of fluctuating velocity and scalar gradients in turbulence. *Exp. Fluids* **53** (4), 925–942.

Hearst, R. J. & Lavoie, P. 2015 The effect of active grid initial conditions on high Reynolds number turbulence. *Exp. Fluids* **56** (10), 185.

Hutchins, N., Nickels, T. B., Marusic, I. & Chong, M. S. 2009 Hot-wire spatial resolution issues in wall-bounded turbulence. *J. Fluid Mech.* **635**, 103–136.

Ishihara, T., Kaneda, Y. & Hunt, J. C. R. 2013 Thin shear layers in high Reynolds number turbulence – DNS results. *Flow Turb. Comb.* **91**, 895–929.

Kwon, Y. S., Philip, J., de Silva, C. M., Hutchins, N. & Monty, J. P. 2014 The quiescent core of turbulent channel flow. *J. Fluid Mech.* **751**, 228–254.

Meinhart, C. D. & Adrian, R. J. 1995 On the existence of uniform momentum zones in a turbulent boundary layer. *Phys. Fluids* **7** (4), 694–696.

Mizuno, Y. & Jiménez, J. 2013 Wall turbulence without walls. *J. Fluid Mech.* **723**, 429–455.

Nedić, J. & Tavoularis, S. 2016 Energy dissipation scaling in uniformly sheared turbulence. *Phys. Rev. E* **93** (3), 033115.

Sekimoto, A., Dong, S. & Jiménez, J. 2016 Direct numerical simulation of statistically stationary and homogeneous shear turbulence and its relation to other shear flows. *Phys. Fluids* **28** (035101).

Vanderwel, C. & Tavoularis, S. 2011 Coherent structures in uniformly sheared turbulent flow. *J. Fluid Mech.* **689**, 434–464.